

**Computation of the dynamic critical exponent of the three-dimensional Heisenberg model**A. Astillero *Departamento de Tecnología de los Computadores y las Comunicaciones, Universidad de Extremadura, 06800 Mérida, Spain  
and Instituto de Computación Científica Avanzada (ICCAEx), 06071 Badajoz, Spain*J. J. Ruiz-Lorenzo *Departamento de Física, Universidad de Extremadura, 06071 Badajoz, Spain;  
Instituto de Computación Científica Avanzada (ICCAEx), Universidad de Extremadura, 06071 Badajoz, Spain;  
and Instituto de Biocomputación y Física de Sistemas Complejos (BIFI), 50018 Zaragoza, Spain*

(Received 13 June 2019; published 16 December 2019)

Working in and out of equilibrium and using state-of-the-art techniques we have computed the dynamic critical exponent of the three-dimensional Heisenberg model. By computing the integrated autocorrelation time at equilibrium, for lattice sizes  $L \leq 64$ , we have obtained  $z = 2.033(5)$ . In the out-of-equilibrium regime we have run very large lattices ( $L \leq 250$ ) obtaining  $z = 2.04(2)$  from the growth of the correlation length. We compare our values with that previously computed at equilibrium with relatively small lattices ( $L \leq 24$ ), with that provided by means a three-loops calculation using perturbation theory and with experiments. Finally we have checked previous estimates of the static critical exponents,  $\eta$  and  $\nu$ , in the out-of-equilibrium regime.

DOI: [10.1103/PhysRevE.100.062117](https://doi.org/10.1103/PhysRevE.100.062117)**I. INTRODUCTION**

The study of the dynamics in and out of equilibrium in a critical phase is of paramount importance since it permits one to extract the critical exponents of the system, hence, to characterize its universality class. In the last decades a great amount of work, analytical, numerical, and experimental, has been devoted to study these issues.

One of the most studied systems has been the three-dimensional (isotropic) classical Heisenberg model. This model plays an important role in magnetism. For example, the Heisenberg universality class describes the paramagnetic-ferromagnetic phase transition of Ni, EuO, and EuS, among others, and some paramagnetic-antiferromagnetic phase transitions such as that of RbMnF<sub>3</sub> [1]. This universality class also characterizes the critical properties of an isotropic Heisenberg model with site-diluted disorder [1,2].

The dynamics of this model has been studied by means of analytical computations [3], numerical simulations at equilibrium [4], and experiments [5,6].

Analytically, the dynamic critical exponent,  $z$ , has been computed using field theory by studying its Model A dynamics (pure relaxational dynamics in which the order parameter is not conserved) [7–9]. A three-loops computation reported in Ref. [3] provided  $z = 2.02$ . This result was extended to four loops in Ref. [10] obtaining  $z = 2.026$  [11].<sup>1</sup> Finally, using nonperturbative renormalization group,  $z = 2.021$  and  $z =$

$2.025$  were computed depending of the frequency regulator used in the computation [11].

Numerically, the equilibrium dynamics of this model was also studied in Ref. [4], and  $z = 1.96(6)$  was reported. The authors were aware that this exponent was slightly below the analytical computation of Ref. [3] and discuss in the paper different systematic bias, for example, a relatively narrow range of the lattice sizes, and despite the accuracy of their values for the correlation times, a more precise determination of these times was needed to study the corrections to the scaling presented in the model.

Finally, from the experimental side, the situation is complicated due to the crossover from the Heisenberg universality class to the dipolar one, which induces a change from  $z \sim 2.5$  (Heisenberg with conserved magnetization and reversible forces, model J [7–9]) to  $z \sim 2$  (dipolar) [5,6]. In particular using perturbed angular correlations of  $\gamma$ -ray spectroscopy Hohenemser *et al.* found  $z = 2.06(4)$  [6] for Ni and  $z \simeq 2$  for Fe; Dunlap *et al.* [12] using electronic spin resonance found  $z = 2.04(7)$  for EuO; and  $z = 2.09(6)$  was found by Bohn *et al.* for EuS [13] using inelastic neutron scattering. It seems that the interplay of spin dipoles with orbital angular momentum or dipolar interactions breaks the conservation of the magnetization on these materials, producing a crossover between Heisenberg model J ( $z \sim 2.5$ ) and Heisenberg model A ( $z \sim 2$ ) [5,6].

Recently Pelissetto and Vicari [14] have used the value provided by field theory in the scaling analysis of their numerical data to study the off-equilibrium behavior of three-dimensional  $O(N)$  models driven by time-dependent external fields and assigned it an error of 0.01, so  $z = 2.02(1)$ , to take into account the uncertainty on the extrapolation to  $\epsilon = 1$  of the three-loops-expansion result.

<sup>1</sup> $z = 2 + c\eta$ ,  $c = 0.726 - 0.137\epsilon + 0.249\epsilon^3 + O(\epsilon^3)$ , where  $\eta$  is the anomalous dimension of the field (from static) and  $\epsilon = 4 - d$ ,  $d$  being the dimensionality of the model.

Consequently, it is of paramount importance to obtain an accurate value for this dynamic critical exponent, in order to be used in future numerical analysis and experiments, and to check the accuracy of the three-loops analytical computation. The main goal of our study is to improve the value of  $z$  using numerical simulations by studying the dependence of the integrated correlation time in the equilibrium regime and the behavior of the correlation length, susceptibility, and energy with the simulation time in the out-of-equilibrium region. In this way, we can compare the performance of equilibrium and out-of-equilibrium methods in the computation of the dynamic critical exponent.

In the equilibrium part of the paper we compute the integrated correlation time, avoiding some of the problems which appear in the computation of the exponential one (e.g., we assume that the autocorrelation function is a single exponential function [15–17]).

In the last two decades, the correlation length has played an important role in both out-of-equilibrium numerical simulations [18–22] and experiments [23] in spin glasses. Due to this, powerful numerical techniques have been developed to compute this observable with high accuracy, which has allowed a precise determination of the dynamic critical exponent just at the critical point as well as inside the critical spin glass phase [21]. We apply these techniques to the three-dimensional (nondisordered) Heisenberg model. In addition to the computation of the dynamic critical exponent, we have checked the consistency of previous and very accurate determinations of the static critical exponents ( $\nu$  and  $\eta$ ) in the out-of-equilibrium regime [24]. Our starting point will be the (very precise) critical temperature computed in Ref. [25] and the static critical exponents reported in Refs. [26,27].

We have also measured the dynamic critical exponent from the decay of the energy at criticality. This decay has also been studied in the past in finite dimensional spin glass [18] and recently has played a central role together with the behavior of the correlation length in the analysis of the Mpemba effect, a striking memory effect [22].

The structure of the paper is the following. In the next section we introduce the model and the observables. In Sec. III we describe our numerical results: in Sec. III A we report the equilibrium determination of  $z$  via the integrated autocorrelation time; in Sec. III B we study the dependence of the correlation length with time and the computation of  $z$  out of equilibrium; and in Secs. III C and III D the correlation function and the energy have been studied, respectively. Section IV is devoted to the conclusions. Two appendices close the paper, one to describe our implementation of GPU and the last to describe how we have computed the statistical error of the exponents with highly correlated data.

## II. THE MODEL AND OBSERVABLES

The Hamiltonian of the three-dimensional Heisenberg model is

$$\mathcal{H} = - \sum_{\langle r, r' \rangle} \mathbf{S}_r \cdot \mathbf{S}_{r'}. \quad (1)$$

$\mathbf{S}_r$  is a classical three component spin on the site  $\mathbf{r}$  of a three-dimensional cubic lattice with volume  $V = L^3$  and

periodic boundary conditions. Without loss of generality we will assume that the spins are unit vectors. The sum runs over all pairs of nearest neighbors spins. We have simulated this model with the standard Metropolis algorithm,<sup>2</sup> and we have run in CPU (smaller time simulations) and GPU (for larger time simulations). Details on the simulations can be found in Appendix A.

### A. Equilibrium

We address the problem of the computation of the dynamic critical exponent in the equilibrium regime by means the computation and further analysis of the integrated autocorrelation time as a function of the lattice size.

We compute for a given observable  $\mathcal{O}(t)$ , the autocorrelation function (we follow Refs. [15,28,29]):

$$C_{\mathcal{O}}(t) \equiv \langle \mathcal{O}(s)\mathcal{O}(t+s) \rangle - \langle \mathcal{O}(t) \rangle^2 \quad (2)$$

and its normalized version

$$\rho_{\mathcal{O}}(t) \equiv C_{\mathcal{O}}(t)/C_{\mathcal{O}}(0). \quad (3)$$

The integrated autocorrelation time is given by

$$\tau_{\text{int},\mathcal{O}} = \frac{1}{2} + \sum_{t=0}^{\infty} \rho_{\mathcal{O}}(t). \quad (4)$$

In a run with  $N$  measurements, the number of independent measurements of the observable  $\mathcal{O}$  is just  $N/(2\tau_{\text{int},\mathcal{O}})$  [15,28,29]. If the number of measurements is finite, for large times  $t$  the noise will dominate the signal in  $\rho_{\mathcal{O}}(t)$ , and to bypass this problem we use the following self-consistent method to compute the integrated time

$$\tau_{\text{int},\mathcal{O}} = \frac{1}{2} + \sum_{t=0}^{c\tau_{\text{int},\mathcal{O}}} \rho_{\mathcal{O}}(t), \quad (5)$$

where  $c$  is usually taken to be 6 or bigger [15,28,29].

At the critical point the integrated autocorrelation time of a long distance observable diverges with the size of the system [17]

$$\tau_{\text{int},\mathcal{O}} \sim L^z [1 + O(L^{-\omega})], \quad (6)$$

where  $z$  is the dynamic critical exponent and  $\omega$  is the leading correction-to-scaling exponent (the leading irrelevant eigenvalue of the theory).

Another time, the exponential correlation time, is defined as

$$\tau_{\text{exp},\mathcal{O}} \equiv \limsup_{t \rightarrow \infty} \frac{-t}{\ln \rho_{\mathcal{O}}(t)}, \quad (7)$$

<sup>2</sup>In the equilibrium simulations, Sec. III A, we have used the Metropolis algorithm proposing a random spin in the unit sphere. In the out-of-equilibrium simulations we have used the Metropolis algorithm in the standard way [28]: we modify the original spin by adding a random vector and normalizing the final vector to the unit sphere. The magnitude of the random vector is selected in order to maintain an acceptance between 40% and 60%. Both versions of the Metropolis algorithm belong to the same dynamic universality class [15].

which also depends on the observable used to define  $\rho_{\mathcal{O}}(t)$ . The exponential autocorrelation time controls the approach to the equilibrium [15].

Once we have defined the exponential correlation function we can write the general scaling form for the correlation function [15]

$$\rho_{\mathcal{O}}(t) = t^{-p_{\mathcal{O}}} f_{\mathcal{O}} \left[ \frac{t}{\tau_{\text{exp},\mathcal{O}}}, \frac{\xi(L)}{L} \right], \quad (8)$$

where  $\xi(L)$  is the equilibrium correlation length computed on a system of size  $L$ . Integrating Eq. (8) in time, we obtain the integrated correlation time and that  $\tau_{\text{int}} \sim \tau_{\text{exp}}^{1-p_{\mathcal{O}}}$ . Both times are proportional if and only if  $p_{\mathcal{O}} = 0$ , and in this situation  $z$  is the same for both times. Otherwise,  $p_{\mathcal{O}} \neq 0$ , and  $\tau_{\text{exp}}$  and  $\tau_{\text{int}}$  will provide with different dynamic critical exponents. See also the discussion of Ref. [17].

In this paper we will use the slowest mode provided by the nonlocal operator  $\mathcal{O} = \mathbf{M}^2$ , where the magnetization  $\mathbf{M}$  is defined as

$$\mathbf{M} = \sum_x \mathbf{S}_x. \quad (9)$$

### B. Out of equilibrium

We have focused on only one local observable, the energy, defined as

$$e(t) = \frac{\langle \mathcal{H} \rangle_t}{V}. \quad (10)$$

We denote the average over different initial conditions at the Monte Carlo time  $t$  by  $\langle (\dots) \rangle_t$ . The renormalization group predicts [9,28], at the critical point, the following behavior for this observable:

$$e(t) = e_{\infty} + Ct^{(d-1/\nu)/z} (1 + At^{-\omega/z}), \quad (11)$$

where  $d$  is the dimensionality of the space (three in this study) and  $\nu$  is the critical exponent which controls the divergence of the equilibrium correlation length. The other two exponents  $z$  and  $\omega$  have been defined in the previous subsection.

One of the main observables on this paper is the correlation function defined as

$$C(r, t) = \frac{1}{V} \sum_x \langle \mathbf{S}_x \mathbf{S}_{r+x} \rangle_t, \quad (12)$$

satisfying, at criticality, the scaling law [9]

$$C(r, t) = \frac{1}{r^a} f \left[ \frac{r}{\xi(t)} \right], \quad (13)$$

which defines the dynamic correlation length,  $\xi(t)$ . As we approach the equilibrium regime,  $\xi(t)$  reaches its equilibrium value.

At the  $d = 3$  critical point and in equilibrium, one should expect

$$C(r, t) \sim \frac{1}{r^{d-2+\eta}} = \frac{1}{r^{1+\eta}}, \quad (14)$$

$\eta$  being the anomalous dimension of the field.

The correlation length  $\xi(t)$  can be estimated by computing [18,19]

$$I_k(t) = \int_0^{L/2} dr r^k C(r, t), \quad (15)$$

by means of

$$\xi_{k,k+1}(t) \equiv \frac{I_{k+1}(t)}{I_k(t)}. \quad (16)$$

We focus in this work on  $\xi_{2,3}$ . On spin glasses was measured  $\xi_{1,2}$  with a correlation function decaying like  $1/r^{0.5}$  [18,19]. In our case, to decrease the weight of the smallest distances we have resorted to compute higher values of  $I_k$ . In Appendix B we describe the detailed procedure we have used to compute the integrals and how we have estimate the statistical error associated with  $\xi_{k,k+1}(t)$ . The dependence of the dynamic correlation length with time is

$$\xi_{k,k+1}(t) \sim t^{1/z} (1 + A_k t^{-\omega/z}). \quad (17)$$

The magnetic susceptibility is given by

$$\chi(t) = \frac{1}{V} \langle \mathbf{M}^2 \rangle_t, \quad (18)$$

or equivalently by

$$\chi(t) = \int d^3x C(|\mathbf{x}|, t). \quad (19)$$

In the regime of large  $\xi(t)$  we recover rotational invariance, and we obtain

$$\chi(t) = 4\pi I_2(t). \quad (20)$$

The temporal dependence of  $\chi(t)$  is

$$\chi(t) \sim t^{(2-\eta)/z} (1 + At^{-\omega/z}), \quad (21)$$

which can be rewritten as

$$\chi(t) \sim \xi_{k,k+1}(t)^{2-\eta} [1 + C_k \xi(t)^{-\omega}]. \quad (22)$$

### III. NUMERICAL RESULTS

In this section we report the computation of the integrated correlation time at equilibrium. After this analysis, we describe our results in the out of equilibrium regime. In particular, we consider the short- and long-time behavior of

TABLE I. Integrated correlation time of  $\mathbf{M}^2$ ,  $\tau_{\text{int},\mathbf{M}^2}$  for  $c = 10$ , as a function of the lattice size,  $L$ . We also report the length of the run at equilibrium,  $n_{\text{sweep}}$ , in units of  $\tau_{\text{int},\mathbf{M}^2}$ . For each lattice size we have performed 50 initial conditions. Notice that all the reported runs satisfy  $n_{\text{sweep}} > 10\,000 \tau_{\text{int},\mathbf{M}^2}$  [15].

$L$	$\tau_{\text{int},\mathbf{M}^2}$	$n_{\text{sweep}}/\tau_{\text{int},\mathbf{M}^2}$
8	24.84(1)	4 122 383
12	53.11(4)	1 928 074
16	93.57(8)	1 094 368
24	211.2(3)	484 848
32	378.3(5)	270 542
48	860(3)	58 333
64	1545(9)	13 782

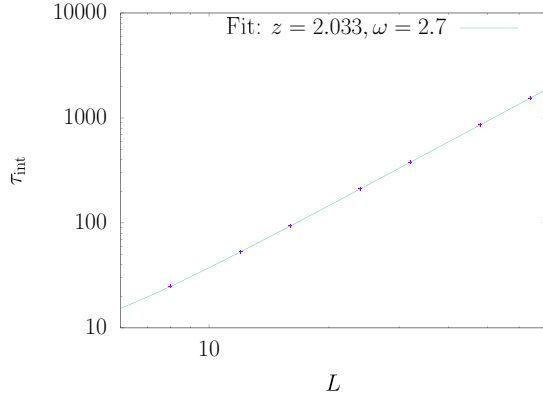


FIG. 1. Behavior of the integrated correlation time,  $\tau_{\text{int},M^2}$ , as a function of the lattice size,  $L$ . We have also shown our best fit taking into account corrections to the scaling (see the text).

correlation length and the long-time behavior of the correlation function and that of the energy. The data are obtained after a sudden quench from  $T = \infty$  to  $T = 1/\beta_c$ . All the numerical simulations were performed at  $\beta_c = 0.693\,001$  [25].

### A. Equilibrium

To obtain the dynamic critical exponent in the equilibrium regime, we compute the integrated correlation time of  $M^2$  when the numerical simulation has reached the equilibrium. We follow the methodology described in Sec. II A, using the self-consistent window algorithm with a window size given by  $c\tau_{\text{int}}$ . We have analyzed the correlation functions with  $c = 6, 8, 10$ , and  $12$ , and we have checked that the  $c = 10$  data are fully compatible with that of  $c = 8$  and  $12$ . We report in the following  $c = 10$  integrated autocorrelation times.

In Table I we report the values of  $\tau_{\text{int},M^2}$  and other parameters of the performed runs. In order to improve the statistics on  $\tau_{\text{int},M^2}$  we have performed 50 independent runs (initial conditions). We have computed the statistical error on the integrated autocorrelation times by using the jackknife method over the independent runs [30,31].

We have fitted  $\tau_{\text{int},M^2}$  to Eq. (6) using  $8 \leq L \leq 64$  obtaining  $z = 2.033(5)$  and  $\omega = 2.7(3)$  with a  $\chi^2/\text{d.o.f.} = 0.36/3$ .<sup>3</sup> We report this fit and the numerical data in Fig. 1. Fitting the data using only a power law (i.e., neglecting the correction-to-scaling term) we obtain a good fit only for  $L \geq 24$  obtaining  $z = 2.026(4)$  with  $\chi^2/\text{d.o.f.} = 0.28/2$ . Both reported values are fully compatible.

Finally we present a scaling analysis of the  $\rho(t)$  function at equilibrium and at the critical point to show that  $\tau_{\text{exp}}$  and  $\tau_{\text{int}}$  are proportional and therefore both times diverge with the same dynamic critical exponent  $z$ . Figure 2 shows the scaling law of the correlation function  $\rho(t)$  as a function of  $t/\tau_{\text{int}}(L)$  instead of  $t/\tau_{\text{exp}}(L)$ , as stated in Eq. (8). Scaling in the new variable holds if and only if  $\tau_{\text{exp}} \propto \tau_{\text{int}}$ , and this is the case apart from small scaling corrections on the  $L \leq 16$  data induced by the term  $\xi(L)/L$  in the scaling function  $f_{\mathcal{O}}$  of

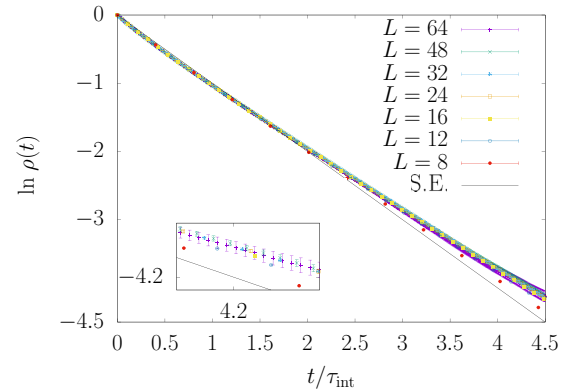


FIG. 2. Behavior of the integrated correlation function,  $\rho(t)$ , for the squared magnetization as a function of  $t/\tau_{\text{int}}(L)$ . Inset: We show a zoom of the long-time region of the main plot, drawing only a small number of points, so the reader can see in a better way the differences among the different lattice sizes. Notice that all the data with  $L \geq 16$  collapse in the scaling formula, and this fact provides a numerical verification of the proportionality of the integrated and exponential correlation times. We have also plotted a single pure exponential (denoted SE),  $\exp(-x)$ , to show that the correlation function is not a single exponential.

Eq. (8); see also the inset of this figure for a detailed and more quantitative view of this effect.

In Ref. [4] the (biggest) exponential correlation time was computed for the magnetization  $\sqrt{M^2}$ . However, the computation of this exponential time is very involved in the case the autocorrelation function  $\rho(t)$  does not show a single exponential decay [14,16]: in Fig. 2 we have plotted a single exponential decay, and the correlation function clearly departs from this behavior.

### B. Correlation length: Shorter times

We report in Fig. 3 the behavior of  $\xi_{23}$  as a function of time for different lattice sizes that we have been able to thermalize. The  $\xi_{23}$ -plateaus obtained for the largest times are

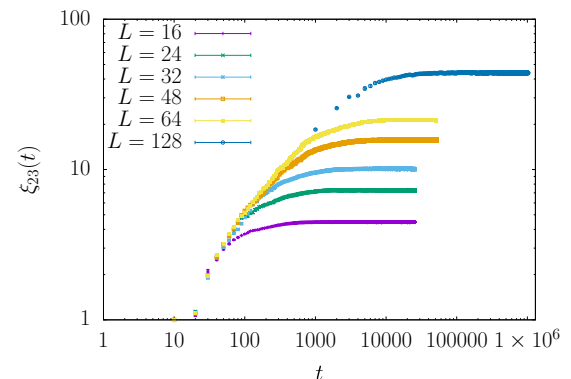


FIG. 3. Behavior of the dynamic correlation length for  $L = 16, 24, 32, 48, 64$  and  $L = 128$ . We have only plotted simulations in which the equilibrium regime has been reached: notice the clear plateau of the different correlation length curves.

<sup>3</sup>In this case, the data for different lattice sizes are not correlated, and we can safely use the diagonal covariance matrix.

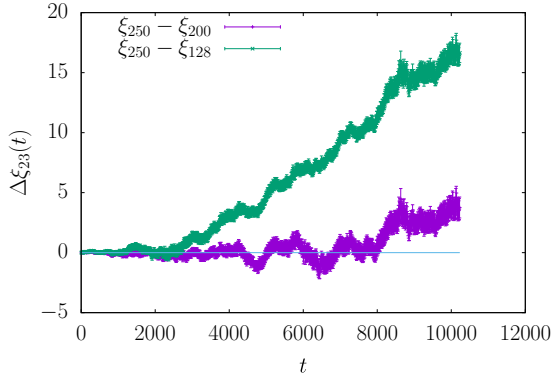


FIG. 4. We show the difference of dynamic correlation lengths,  $\Delta\xi_{23}(t)$ , for three pairs of lattice sizes as a function of time:  $\xi_{L=250} - \xi_{L=200}$  and  $\xi_{L=250} - \xi_{L=128}$ . The zero value has been marked with a horizontal line. Notice that the  $L = 250$  data are asymptotic (as compared with those of  $L = 200$ ) for  $t < 8100$  (the data lie, at most, at one standard deviation of the zero value).

clear evidence that the numerical simulations have reached the equilibrium.

In order to extract the dynamic critical exponent by using Eq. (17), we need to work in the out-of-equilibrium regime, avoiding the transient regime and the equilibrium domain. Therefore, we need to check the following points. Firstly, we need to avoid the transient regime between the power law behavior (pure out-of-equilibrium regime) and the plateau one (equilibrium one). Secondly, Eq. (17) holds after the initial transient of the dynamics. Therefore, we need to fix a minimum time  $t_{\min}$ . And finally, in order to avoid finite size effects, we need to compare the correlation lengths for different lattice sizes.

In this section we have performed numerical simulations with  $t < 10\,240$  (in order to avoid the transient and equilibrium regimes). We have simulated 4000 random initial conditions for  $L = 128$  and  $L = 200$  and 5325 initial conditions for  $L = 250$ .

In Fig. 4 we have plotted, to check finite size effects, the differences among the correlation lengths of  $L = 128$  and 200 and that of 250. In this figure we can see that the data of the

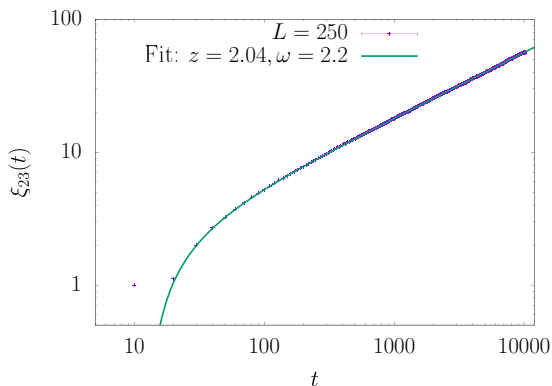


FIG. 5. Behavior of the dynamic correlation length for  $L = 250$  in the out-of-equilibrium regime. The fit is only for the  $L = 250$  data in the region  $100 \leq t < 8100$ .

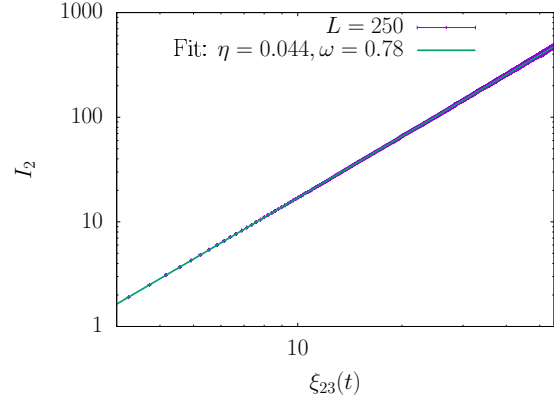


FIG. 6. Behavior of  $I_2(\xi_{23}) \propto \chi$  for  $L = 250$ . We also plot the fit taking into account scaling corrections but with the  $\omega$  exponent fixed to the equilibrium value as described in the text.

$L = 200$  and  $L = 250$  lattices are compatible in the statistical error for  $t < 8100$ .

From the previous discussion we must fit the data for  $\xi_{23}$  in the time interval given by  $t \in [t_{\min}, 8100]$  using the  $L = 250$  data:  $t_{\min}$  being the smallest value of the Monte Carlo time that provides a good  $\chi^2/\text{d.o.f.}$  (e.g.,  $\sim 1$ ) by fitting the data to Eq. (17).

In Fig. 5 we show the behavior of  $\xi_{23}$  for the largest lattice size simulated in this time regime,  $L = 250$ . By fitting  $L = 250$  data in the interval  $t \in [100, 8100]$  we have obtained  $z = 2.04(2)$  and  $\omega = 2.2(4)$  with  $\chi^2/\text{d.o.f.} = 287/796$ . Furthermore, we can report that a fit neglecting the contribution of the correction-to-scaling term provides  $z = 2.012(13)$  with  $t \in [400, 8100]$  and  $\chi^2/\text{d.o.f.} = 361/768$ . Both reported values are statistically compatible.

We have computed the statistical error on the  $z$  exponent with the jackknife method [30,31]. As described in Appendix B, we compute the  $\chi^2$  using a diagonal covariance matrix (neglecting the correlations of the data), but we use a jackknife procedure to take into account the (important) different correlations among the data. Hence, in the following all  $\chi^2$  are computed assuming a diagonal covariance matrix; we refer the reader to Appendix B for a discussion of the interpretation of this *diagonal*  $\chi^2$  and for more details on the procedure we have followed to take into account the correlation among the data (in time or in distance; see below) and the way we have computed the statistical errors on the values of the critical exponents.<sup>4</sup>

Having computed  $\xi_{23}$  and  $I_2 \propto \xi_{23}^{2-\eta}$  we can, as a check, estimate the  $\eta$  exponent. Figure 6 shows  $I_2$  as a function of  $\xi_{23}$ . We can compute  $\eta$  using the time interval  $t \in [100, 8100]$  obtaining  $\eta = 0.029(20)$  and  $\omega = 0.8(4)$  with  $\chi^2/\text{d.o.f.} =$

<sup>4</sup>The same fit performed with the help of Gnuplot [32] (with a diagonal covariance matrix) provides a  $z = 2.012$  with an asymptotic error of 0.00075. In order to obtain the right statistical error, we need to divide this asymptotic error by  $\sqrt{\chi^2/\text{d.o.f.}} = 0.687$  [31], obtaining the final value of  $z = 2.012(1)$ . Notice that the computed error discarding correlations among the different times is a factor 13 times smaller.

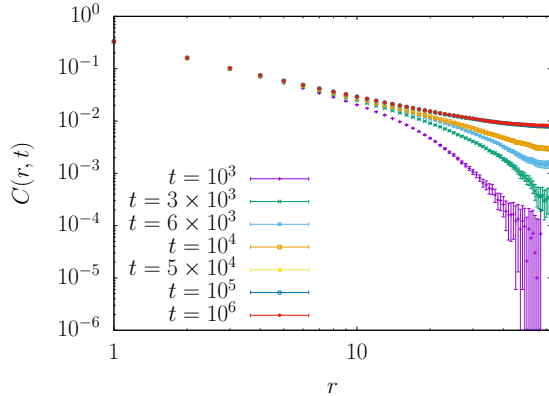


FIG. 7. Correlation function at criticality for a  $L = 128$  lattice. We have drawn different times in order to show the crossover between the out-of-equilibrium region and the equilibrium one. Notice the bad signal-to-noise ratio in the tail of  $C(r, t)$  for large  $r$  and shorter times  $t$ , and how this ratio improves with time, generating a plateau (due to the periodic boundary conditions) with small error.

342/796. In this case the  $\omega$  exponent is similar to the equilibrium value  $\omega \simeq 0.78$  [33,34]. We can improve the value of  $\eta$  by fixing the correction-to-scaling exponent  $\omega$  to the equilibrium value  $\omega = 0.78$ , obtaining  $\eta = 0.044(7)$  with  $\chi^2/\text{d.o.f.} = 666/757$  ( $t \in [50, 8100]$ ). Our value compares very well (but with 20 times more error) with that computed at equilibrium:  $\eta = 0.0378(3)$  [26,27]. Finally, neglecting the correction-to-scaling term, we have found  $\eta = 0.043(6)$  with  $\chi^2/\text{d.o.f.} = 676/768$  ( $t \in [400, 8100]$ ). All three reported values are statistically compatible.

### C. Correlation function for larger times

In Fig. 7 we plot  $C(r, t)$  for different times using  $L = 128$  data (200 initial conditions) and very long times. One can see the crossover of the dynamic correlation function between the off-equilibrium regime and the equilibrium one. In Appendix B we provide more details about the functional form of  $C(r, t)$  in the out-of-equilibrium regime. We can also check that we have reached the equilibrium regime by plotting the behavior of  $\xi_{23}(t)$  (see  $L = 128$  curve of Fig. 3). This nonlocal

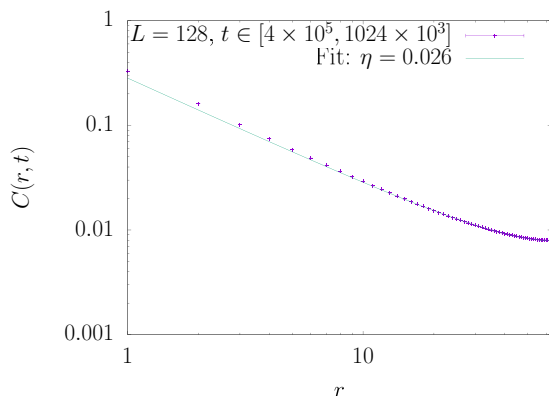


FIG. 8. Equilibrium correlation function at criticality for a  $L = 128$  lattice. The continuous line is a fit to Eq. (23) with  $\eta = 0.026$ .

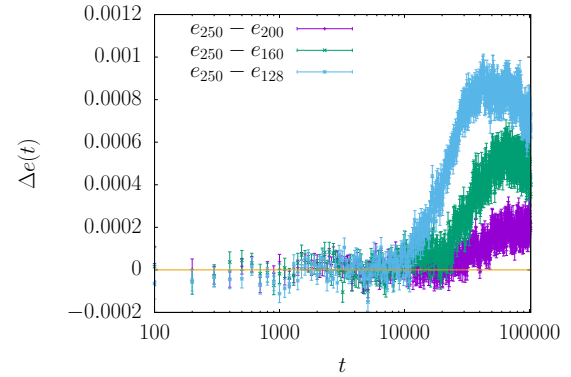


FIG. 9. We show the difference of energies,  $\Delta e(t)$  for three pairs of lattice sizes as a function of time:  $e_{L=250} - e_{L=200}$ ,  $e_{L=250} - e_{L=160}$ , and  $e_{L=250} - e_{L=128}$ . The zero value has been marked with a horizontal line. Notice that the  $L = 250$  data are asymptotic (as compared with those of  $L = 200$ ) for  $t < 48\,000$  (the data are at one standard deviation of the zero value).

observable has clearly reached its equilibrium (plateau) value. We can safely assume that for  $t > 4 \times 10^5$  we have thermalized the  $L = 128$  lattice, and we can try to extract the value of the anomalous dimension by averaging the correlation function above this time.

The analytical behavior at the critical point in this regime (large  $L$ ) is given by Eq. (14). Bearing in mind that we are using periodic boundary conditions, we can write the following improved equation to fit our numerical data:

$$C(r, L) = \frac{A}{r^{1+\eta}} + \frac{A}{(L-r)^{1+\eta}}. \quad (23)$$

By fitting the data of Fig. 8 to this functional form, we obtain  $\eta = 0.026(4)$  (by using only  $t > 4 \times 10^5$ ,  $r \geq 16$ , and  $\chi^2/\text{d.o.f.} = 44/48$ ) in a good statistical agreement with the value drawn from equilibrium studies  $\eta = 0.0378(3)$ . We have followed the method described in Appendix B in order to obtain the error in the  $\eta$  exponent.<sup>5</sup>

### D. Energy for larger times

We have analyzed the behavior of the energy at criticality in order to compute the ratio of critical exponents  $(d - 1/\nu)/z$ . To analyze this behavior, we have run  $L = 128$  (153 i.c.) in the following),  $L = 160$  (600 i.c.),  $L = 200$  (684 i.c.), and  $L = 250$  (684 i.c.) for longer times  $t < 102\,400$ .

First, we study in Fig. 9 the effect of a finite size lattice on the values of energy as a function of time. From this figure one can see that it is safe to take fits only in the range  $t < 48\,000$  in order to avoid finite size effects (at least in the precision of our simulation).

In Fig. 10 we show the results for the largest lattice  $L = 250$ . We have fitted the  $L = 250$  data to a power law, in the

<sup>5</sup>The same fit, assuming no correlation among the different values of the correlation function, provides an error of 0.0013, three times smaller than that obtained in our procedure.

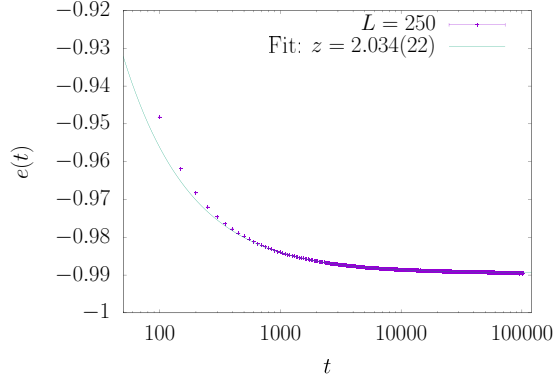


FIG. 10. Behavior of the energy  $e(t)$  at the critical point for the  $L = 250$  run. We also draw the fit in order to extract the ratio  $(d - 1/\nu)/z$  with  $d = 3$ ,  $\nu = 0.7117(5)$  fixed getting  $z = 2.034(22)$ .

time interval  $t \in [1000, 48\,000)$  obtaining  $z = 2.034(22)$  and  $e_\infty = -0.989\,505(17)$ , with a diagonal  $\chi^2/\text{d.o.f.} = 985/939$ . We have fixed in the fit the value  $\nu = 0.7117(5)$  [26,27]. The really small error bar of the  $\nu$  exponent does not have a measurable effect in the final error bar of  $z$ . To finish the analysis of the energy, we have also checked corrections to scaling for this observable, and we have found that the exponent  $\omega_{\text{eff}} = 2 \times 0.78$  describes very well the numerical data obtaining  $z = 2.13(7)$  and  $e_\infty = -0.989\,525(22)$  with  $\chi^2/\text{d.o.f.} = 980/947$ .

#### IV. CONCLUSIONS

By performing in- and out-of-equilibrium numerical simulations we have computed the dynamic critical exponent  $z$ .

The most accurate value has been computed in the equilibrium regime by studying the integrated correlation time as a function of the lattice size:  $z = 2.033(5)$ . We have found a correction-to-scaling exponent  $\omega = 2.7(3)$ . In addition we have provided strong numerical evidence for the proportionality of the integrated and exponential correlation times.

We have also computed the  $z$  exponent in the out-of-equilibrium regime obtaining  $z = 2.04(2)$  and  $\omega = 2.2(4)$ , which is similar to the  $\omega$  exponent computed at equilibrium. Moreover, we have checked the consistency of the computed critical exponents at equilibrium with the out-of-equilibrium ones with and without considering corrections to scaling. The (equilibrium) value of  $\nu$  provides us, by monitoring the energy, with another dynamic exponent estimate ( $z = 2.034(22)$ ) fully compatible with the previous ones.

Furthermore, our value of  $z$  has improved the statistical precision of that computed in numerical simulations performed at equilibrium in relatively small lattices ( $L \leq 24$ ) [4]. Our computed values match very well with that obtained in experiments and with the exponent computed using field theoretical techniques [3,10,11] (although in this framework it is very difficult to assign an uncertainty to this estimate).

#### ACKNOWLEDGMENTS

We thank L. A. Fernandez, M. Lulli, A. Pelissetto, V. Martin-Mayor, J. Salas, J. A. del Toro, and D. Yllanes for

TABLE II. Hardware features of the CPUs and GPUs.

CPU/GPU model	CPU Intel Core i7	GPU Geforce GTX 1080 G1	GPU Tesla K80
Cores	20	2560	4992
Core clock	2.26 GHz	1.86 GHz	0.88 GHz
Total memory	24 GB	8 GB	24 GB
Memory bandwidth	-	-	480 GB/s

discussions. This work was partially supported by Ministerio de Economía y Competitividad (Spain) through Grant No. FIS2016-76359-P and by Junta de Extremadura (Spain) through Grants No. GRU10158 and No. IB16013 (partially funded by FEDER). We have run the simulations in the computing facilities of the Instituto de Computación Científica Avanzada (ICCAEx) and in the CETA-Ciemat; we thank Dr. A. Paz for his support.

#### APPENDIX A: DETAILS OF THE NUMERICAL SIMULATIONS AND GPU PARALLEL IMPLEMENTATION

We have simulated the Heisenberg model using the Metropolis algorithm on CPUs and GPUs (see Table II). We have simulated  $L = 128, 160, 200$ , and  $250$  for more than  $10\,000$  random initial conditions. The GPU code has been programmed in CUDA C [35]. The original C code which simulates the Heisenberg model has been parallelized in three parts:

(1) Computation of the nearest neighbors of each spin: the C code has a loop which goes sequentially through all the spins one by one. However, in the GPU code each spin has associated an execution thread, and all the nearest neighbors of every spin are computed at once.

(2) Metropolis algorithm: in the sequential C code we can find several loops in the Metropolis part. So the parallel GPU code reduces meaningfully the execution time, especially in large systems ( $L \sim 200$ ). Moreover, the lattice has been divided using a checkerboard scheme (Fig. 11) [36]. In this

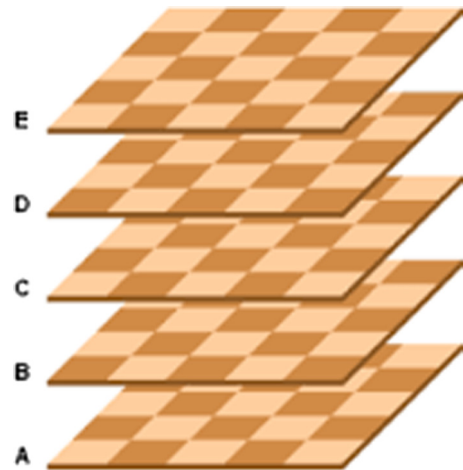


FIG. 11. Division of the three-dimensional lattice using a checkerboard scheme.

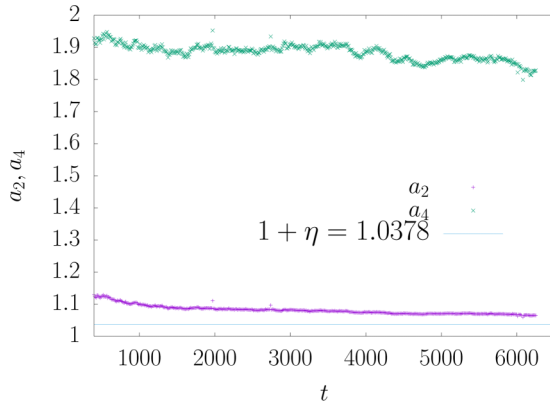


FIG. 12. Behavior of the exponents  $a_2$  and  $a_4$  as a function of time for  $L = 200$ . The horizontal line is the equilibrium theoretical expectation for  $a_2$ :  $1 + \eta = 1.0378$ .

way, the Metropolis algorithm has been executed first of all in the “white” spins and after that in the “black” ones.

(3) Random numbers: to have high-quality random numbers is mandatory in computational physics. Initially, we have used the CURAND random numbers, which are part of the CUDA C distribution [35]. The problems with the CURAND random numbers have appeared when we have performed long simulations using a huge quantity of random numbers. To avoid these problems we have used congruential random numbers [37].

Making use of the GPU Tesla K80 we have achieved a speedup of 22, which represents an important reduction of the execution time.

## APPENDIX B: DETAILS OF THE ANALYSIS OF THE COMPUTATION OF THE CORRELATION LENGTH

We describe the different steps we have followed in order to compute  $\xi(t)$  and its associated exponent  $z$  [18,19,38,39]. The important point of this approach is to avoid the use of the full covariance matrix since this matrix is frequently singular (see, for example, Refs. [38,40]). Thus, our procedure is the following:

(1) We compute using the jackknife method over the set of the initial conditions the statistical error of  $C(r, t)$ , denoted as  $\sigma[C(\Lambda, t)]$ .

(2) To compute  $I_k$  we introduce a cutoff to have a good control of the signal-to-noise ratio of  $C(r, t)$  for large values of  $r$  (see also Fig. 7).

(a) We compute the cutoff  $\Lambda$  using the condition  $\sigma[C(\Lambda, t)] = 4C(\Lambda, t)$ .

(b) For a fixed  $t$  and  $r_{\min} < r < \Lambda$  we fit the correlation function to the functional form given by

$$C(r, t) = \frac{a_1}{r^{a_2}} \exp(-a_3 r^{a_4}). \quad (\text{B1})$$

with  $r_{\min}$  is the minimum value of  $r$ , which provided, for  $C(r, t)$ , a good fit (e.g.,  $\chi^2/\text{d.o.f.} \sim 1$ ) to Eq. (B1). In Fig. 12 we report the dependence of the exponents  $a_2$  and  $a_4$  with the Monte Carlo time. Notice that  $a_2$  converges to the equilibrium value [see Eq. (14)] given by  $1 + \eta = 1.0378$  and  $a_4 \simeq 1.8$ .

(c) We compute the integral in Eq. (15) using the numerical values of the correlation  $C(r, t)$  for  $r < \Lambda$  and using the values provided by the fit [Eq. (B1)] for  $\Lambda < r < L/2$ .

(d) Using the previous procedure, we compute the statistical error of  $\xi(t)$  using again the jackknife method over the set of the initial conditions. The time interval for the fit is decided by imposing a diagonal  $\chi^2/\text{d.o.f.} \sim 1$ .

(e) The jackknifed  $\xi$  are used to compute the jackknifed values of  $z$ , and this allows us to compute the statistical error of the dynamic critical exponent using the standard deviation in the jackknife method. Notice that for extracting  $z$  on each jackknife block, we use the *diagonal* covariance matrix. However, the jackknife procedure reproduces with high accuracy the effect of the correlations among the different times.

Notice that the *diagonal*  $\chi^2/\text{d.o.f.}$  does not have a rigorous interpretation like that of the full (nondiagonal) one. One can show (see the detailed analysis of this procedure carried out in Sec. B.3.3.1 of Ref. [38]) that the *diagonal*  $\chi^2/\text{d.o.f.}$  behaves as if there were a small number of degrees of freedom, hence, one cannot compute confident limits as usual.

Finally, in Ref. [20] was shown that the error bars are essentially equal (using this jackknife procedure, neglecting the correlations among the data) to those obtained taking into account all the statistical correlations among the data.

[1] A. Pelissetto and E. Vicari, *Phys. Rep.* **368**, 549 (2002).  
 [2] A. Gordillo-Guerrero and J. J. Ruiz-Lorenzo, *J. Stat. Mech.: Theory Exp.* (2007) P06014.  
 [3] N. V. Antonov and A. N. Vasilev, *Theor. Math. Phys.* **60**, 671 (1984).  
 [4] P. Peczak and D. P. Landau, *Phys. Rev. B* **47**, 14260 (1993).  
 [5] L. Chow, C. Hohenemser, and R. M. Suter, *Phys. Rev. Lett.* **45**, 908 (1980).  
 [6] C. Hohenemser, L. Chow, and R. M. Suter, *Phys. Rev. B* **26**, 5056 (1982).

[7] P. C. Hohenberg and B. I. Halperin, *Rev. Mod. Phys.* **49**, 435 (1977).  
 [8] R. Folk and G. Moser, *J. Phys. A* **39**, R207 (2006).  
 [9] U. Täuber, *Critical Dynamics: A Field Theory Approach to Equilibrium and Non-Equilibrium Scaling Behavior* (Cambridge University Press, Cambridge, 2017).  
 [10] L. Ts. Adzhemyan, S. V. Novikov, and L. Sladkoff, [arXiv:0808.1347](https://arxiv.org/abs/0808.1347).  
 [11] C. Duclut and B. Delamotte, *Phys. Rev. E* **95**, 012107 (2017).  
 [12] R. A. Dunlap and A. M. Gottlieb, *Phys. Rev. B* **22**, 3422 (1980).

- [13] H. G. Bohn, A. Kollmar, and W. Zinn, *Phys. Rev. B* **30**, 6504 (1984).
- [14] A. Pelissetto and E. Vicari, *Phys. Rev. E* **93**, 032141 (2016).
- [15] A. Sokal, in *Functional Integration*, edited by C. DeWitt-Morette, P. Cartier, and A. Folacci, NATO ASI Series (Series B: Physics) Vol. 361 (Springer, Boston, 1997).
- [16] J. Salas and A. D. Sokal, *J. Stat. Phys.* **85**, 297 (1996).
- [17] M. Hasenbusch, A. Pelissetto, and E. Vicari, *J. Stat. Mech.: Theory Exp.* (2007) P11009.
- [18] F. Belletti, M. Cotallo, A. Cruz, L. A. Fernandez, A. Gordillo-Guerrero, M. Guidetti, A. Maiorano, F. Mantovani, E. Marinari, V. Martin-Mayor, A. Muñoz-Sudupe, D. Navarro, G. Parisi, S. Perez-Gaviro, J. J. Ruiz-Lorenzo, S. F. Schifano, D. Sciretti, A. Tarancon, R. Tripiccione, J. L. Velasco, and D. Yllanes (Janus Collaboration), *Phys. Rev. Lett.* **101**, 157201 (2008).
- [19] F. Belletti, A. Cruz, L. A. Fernandez, A. Gordillo-Guerrero, M. Guidetti, A. Maiorano, F. Mantovani, E. Marinari, V. Martín-Mayor, J. Monforte, A. Muñoz Sudupe, D. Navarro, G. Parisi, S. Perez-Gaviro, J. J. Ruiz-Lorenzo, S. F. Schifano, D. Sciretti, A. Tarancon, R. Tripiccione, and D. Yllanes (Janus Collaboration), *J. Stat. Phys.* **135**, 1121 (2009).
- [20] M. Lulli, G. Parisi, and A. Pelissetto, *Phys. Rev. E* **93**, 032126 (2016).
- [21] M. Baity-Jesi, E. Calore, A. Cruz, L. A. Fernandez, J. M. Gil-Narvion, A. Gordillo-Guerrero, D. Iñiguez, A. Maiorano, E. Marinari, V. Martin-Mayor, J. Moreno-Gordo, A. Muñoz-Sudupe, D. Navarro, G. Parisi, S. Perez-Gaviro, F. Ricci-Tersenghi, J. J. Ruiz-Lorenzo, S. F. Schifano, B. Seoane, A. Tarancon, R. Tripiccione, and D. Yllanes (Janus Collaboration), *Phys. Rev. Lett.* **120**, 267203 (2018).
- [22] M. Baity-Jesi, E. Calore, A. Cruz, L. A. Fernandez, J. M. Gil-Narvion, A. Gordillo-Guerrero, D. Iñiguez, A. Maiorano, E. Marinari, V. Martin-Mayor, J. Moreno-Gordo, A. Muñoz-Sudupe, D. Navarro, G. Parisi, S. Perez-Gaviro, F. Ricci-Tersenghi, J. J. Ruiz-Lorenzo, S. F. Schifano, B. Seoane, A. Tarancon, R. Tripiccione and D. Yllanes (Janus Collaboration), *PNAS* **116**, 15350 (2019).
- [23] S. Guchhait and R. Orbach, *Phys. Rev. Lett.* **112**, 126401 (2014).
- [24] G. Parisi, F. Ricci-Tersenghi, and J. J. Ruiz-Lorenzo, *Phys. Rev. E* **60**, 5198 (1999).
- [25] H. Garcia-Ballesteros, L. A. Fernandez, V. Martin-Mayor, and A. M. Sudupe, *Phys. Lett. B* **387**, 125 (1996).
- [26] M. Campostrini, M. Hasenbusch, A. Pelissetto, P. Rossi, and E. Vicari, *Phys. Rev. B* **65**, 144520 (2002).
- [27] M. Hasenbusch and E. Vicari, *Phys. Rev. B* **84**, 125136 (2011).
- [28] D. J. Amit and V. Martín Mayor, *Field Theory, The Renormalization Group and Critical Phenomena* (World Scientific, Singapore, 2005).
- [29] N. Madras and A. D. Sokal, *J. Stat. Phys.* **50**, 109 (1989).
- [30] B. Efron, *The Jackknife, the Bootstrap, and Other Resampling Plans* (Society for Industrial and Applied Mathematics, Philadelphia, 1982).
- [31] P. Young, [arXiv:1210.3781](https://arxiv.org/abs/1210.3781).
- [32] <http://www.gnuplot.info>.
- [33] R. Guida and J. Zinn-Justin, *J. Phys. A* **31**, 8103 (1998).
- [34] M. Hasenbusch, *J. Phys. A* **34**, 8221 (2001).
- [35] NVIDIA, *NVIDIA CUDA C Programming Guide* (NVIDIA, 2018), [https://docs.nvidia.com/cuda/archive/9.1/pdf/CUDA\\_C\\_Programming\\_Guide.pdf](https://docs.nvidia.com/cuda/archive/9.1/pdf/CUDA_C_Programming_Guide.pdf).
- [36] M. Lulli, M. Bernaschi, and G. Parisi, *Comput. Phys. Commun.* **196**, 290 (2015).
- [37] D. Knuth, *The Art of Computing Programming: Seminumerical Algorithms*, Vol. 2 (Addison Wesley, New York, 1998).
- [38] D. Yllanes, Ph.D. thesis, Universidad Complutense de Madrid, 2011.
- [39] C. Michael, *Phys. Rev. D* **49**, 2616 (1994).
- [40] D. Seibert, *Phys. Rev. D* **49**, 6240 (1994).